Science, Engineering and Technology Vol. 6, No. 1, pp. 25-38
www.setjournal.com https://doi.org/10.54327/set2026/v6.i1.340

Analysis of Vibro-Impact System with Ideal Excitation and Various Friction Models

Kanita Lemeš, Džanko Hajradinović, Zlata Jelačić

University of Sarajevo – Faculty of Mechanical Engineering, Vilsonovo šetaliste 9, Sarajevo, 71000, Bosnia and Herzegovina.

Abstract

In this paper, the dynamic analysis of a vibro-impact system with ideal excitation and various friction models is performed. A physical model of an oscillating mechanical system with possible impact occurrence is presented and the corresponding mathematical model is derived by using Lagrange's equations of motion. To describe interaction between impact element and environment, three different friction models are considered: Coulomb, viscous and Coulomb-Stribeck model. Newton's impact law with a coefficient of restitution is employed to describe relationship between pre-impact and post-impact velocities. The dynamic behavior of the vibro-impact system under the ideal excitation, where the system does not influence the excitation source, is investigated for each friction model by numerically solving the governing equations. The results of numerical analysis are presented through amplitude-frequency diagrams, displacement-time responses and phase portraits. The main objective is to determine the influence of different friction models on amplitude-frequency diagrams, particularly on the regions exhibiting impact and non-impact behavior. For parameter regions with multiple coexisting solutions, basins of attraction are constructed to illustrate the dependence of the system regime on initial conditions.

Keywords*:* vibro-impact, friction models, ideal excitation, dynamic response.

1. Introduction

Vibro-impact systems are widely used in engineering applications, such as mechanical, civil and geotechnical engineering, where intermittent contact or repetitive impact motion may be intentionally utilized or may occur during system operation. These systems are used in many devices, including impact dampers for vibration suppression in machinery or structures, percussive tools and drilling systems, impact crushers and milling equipment in material processing, as well as vibratory pile driving devices and systems for soil compaction and ground improvement.

Such systems typically consist of an impact element driven by a drive mechanism and elastic elements that transfer motion from the drive mechanism to the impact element. When the system does not influence the excitation source, as considered in this study, the excitation is referred to as ideal. Otherwise, the excitation is non-ideal, meaning that the excitation source influences the system while the system simultaneously affects the excitation source.

The analysis of vibro-impact systems is challenging due to their strong nonlinearity and non-smooth characteristics. The presence of impacts introduces velocity discontinuities, while friction, as a highly complex physical phenomenon, further contributes to the nonlinear dynamic behavior of the system. As a result, vibro-impact systems may exhibit complex responses, including different motion regimes and sensitivity to initial conditions. In order to predict the dynamic behavior of a vibro-impact system, an appropriate friction model

Corresponding author: Kanita Lemeš (kanita.lemes@mef.unsa.ba)
Received: 17 February 2026; Revised: 12 March 2026; Accepted: 16 March 2026; Published: 1 April 2026

must be selected, since the presence of friction is inevitable in real vibro-impact systems. Differences in motion regimes, oscillation amplitudes, impact velocities, and the number of impacts may be noticeable depending on the friction model used to describe the interaction between elements of the vibro-impact system or their interaction with the surrounding environment. Therefore, the analysis of the influence of different friction models represents an important step toward a better understanding of the complex dynamic behavior of vibro-impact systems that are widely used in many different engineering applications.

An analysis of nonlinear oscillatory mechanical systems with two degrees of freedom and various friction models has been reported in [1]. Three friction models — Coulomb, viscous, and Coulomb–Stribeck — have been employed to describe the interaction between the impact element and the horizontal surface, and are described in [2] and [3]. The behavior of vibro-impact systems with non-ideal excitation has been studied in [4], [5], [6] and [7]. In [4], the influence of stall torque on the system dynamics is analyzed, and the results indicate that non-ideal excitation with sufficiently high stall torque behaves similarly to ideal excitation. The numerical and analytical study presented in [5] includes an inelastic impact model, which is also adopted in the present work.

Numerical and experimental investigations of capsule-type vibro-impact systems have been presented in [8], [9], [10], [11] and [12], highlighting their potential applications in inspection and biomedical engineering. The capsule systems analyzed in these studies were driven by ideal excitation. Reference [8] focuses on the influence of different friction models on capsule response, while [9] includes system modeling, bifurcation analysis, and energy consumption evaluation. Experimental validation of the capsule model is reported in [10] and [11]. Optimization of the amplitude and frequency of ideal excitation to achieve desired motion under different environmental conditions is investigated in [12].

Effect of friction on vibro-impact locomotion system, modeled as capsule, similar to the models in [8], [9], [10], [11], [12], was studied in [13] and [14]. The focus is on the influence of the friction force level on dynamic response of the vibro-impact system. Bifurcation analysis and basin of attraction are presented in [13] and the results showed that friction level can affect regime of the system, whether the motion would be periodic or chaotic. Research [14] focuses, not only on the vibro-impact locomotion system under the various friction levels, but also on the pure vibration driven system.

Duffing oscillator, as purely oscillating and as vibro-impact system, is analyzed in [15]. Excitation of the system is non-ideal, as in [4], [5], [6], [7]. The analysis focused on the influence of the constraint on the system attractors, examining whether it suppresses or modifies their structure. Numerical results indicate that, although the attractor may remain largely unchanged, the associated basin of attraction can undergo significant transformation.

Bifurcation analysis of the vibro-impact system with ideal excitation is performed in [16], [17] and [18]. Vibro-impact drilling system was analyzed in [16], while vibro-impact experimental rig with two-sided constraint in [17], numerically and experimentally. As a result of bifurcation analysis, Hopf bifurcation, period doubling bifurcation and chaotic motion of the vibro-impact system with two degrees of freedom was observed in [18]. The main difference between [18] and previously mentioned studies is that [18] considered vibro-impact system with fractional-order derivative.

Chaos control in the mechanical system was studied in [19], [20], [21] and [22]. Systems with ideal excitation were analyzed in [19], [20] and [21]. Application of the linear vibration absorber in order to suppress chaos in nonlinear oscillator was studied in [19]. Implementation of the damping control law for chaos control in impact oscillator was studied in [20]. As for the research [21], the main difference from the previously mentioned studies, is the analysis of the plastic impact oscillator. Controlling chaos in system with non-ideal excitation by impact dampers was studied in [22].

Experimental study on vibro-impact system is done in [23], [24] and [25]. In references [23] and [24] vibro-impact system with single degree of freedom is analyzed by numerical simulations, as well as by experimental studies. Focus of study [24] is the influence of the gap size on dynamic response of the system. Difference of the analysis in [25] is the employed impact model, in which study is performed for viscoelastic and Hertzian contact. Presence of the multiple periodic, quasi-periodic and chaotic attractors in case of the vibro-impact system with

complex impact model is confirmed based on numerical and experimental results.

Influence of the impact model on the dynamic response of the vibro-impact system with ideal excitation is analyzed in [26]. Hard and soft impact models were implemented with parameters for which the models were equivalent in energy dissipation.

The application of data-driven and machine learning approaches for analyzing the dynamic behavior of complex engineering systems has attracted increasing attention in recent years. Numerical simulations, particularly in cases involving computationally expensive nonlinear analysis, are applied alongside the previously mentioned approaches. Reference [27] proposed a learning model, based on nonlinear numerical simulations, for predicting the seismic response of the vehicle-bridge interaction. The results of this study demonstrated that by applying machine learning models, high prediction accuracy can be achieved, while significantly reducing computational cost. Such approaches show promising directions for future research and performance prediction, especially in problems involving complex nonlinear dynamical systems.

In previous studies vibro-impact systems with different friction models have been investigated. However, the qualitative and quantitative influence of the friction models on the dynamic behavior of the vibro-impact system with ideal excitation has not been clarified, which is the main contribution of the research performed in this paper. Therefore, the goal of the present study is to analyze the influence of three friction models: Coulomb, viscous, and Coulomb–Stribeck on the dynamic response of a vibro-impact system with ideal excitation. The analysis includes the identification of non-impact and impact regimes, as well as the multiple solution regions, that are commonly observed in vibro-impact systems. The main contribution of this analysis is to clarify the role of the friction model in vibro-impact systems.

The paper is organized as follows. Section 2 presents the physical model of the single-degree-of-freedom vibro-impact system, together with the formulation of the implemented friction models. The mathematical model is derived using Lagrange's equations of motion for each friction case. Section 3 presents numerical results and a comparative analysis of system responses under different friction models. The influence of friction on the dynamic behavior is examined through amplitude-frequency diagrams, basins of attraction, displacement–time responses, and phase portraits. Concluding remarks are provided in Section 4.

2. Physical and Mathematical Modelling

In this work, the vibro-impact system shown in Figure 1 is analyzed. The system consists of an impact element B with mass m_B, a piston element A with mass m_A, and a drive mechanism. The piston element interacts with the impact element B via a linear spring with stiffness c. The contact surface between the piston element and the supporting horizontal surface is assumed to be frictionless. The impact surface is located on the right side of the impact element. The drive mechanism consists of an electric motor, connecting bars, and the piston element. The motion generated by the drive mechanism is transmitted to the piston and the impact element. The excitation of the system is considered ideal, meaning that the system does not influence the excitation source. Consequently, the angular velocity of the electric motor remains constant. The driver link $\overline{OD}$, with length r and moment of inertia J_O about the rotational axis through point O, is connected to the electric motor and performs rotational motion. Link $\overline{OD}$ is connected to bar $\overline{CE}$ via a weightless slider at point D. Bar $\overline{CE}$, with length l_2 and moment of inertia J_2 about point C, performs rotational motion. The distance between points O and C is denoted by l_1. Bar $\overline{EA}$ is connected at one end to bar $\overline{CE}$ via a joint and at the other end to the piston element. Bar $\overline{EA}$, with length l_3, mass m_3, and moment of inertia J_3 about its center of mass, undergoes planar motion. In this analysis, an inelastic impact model with a coefficient of restitution – hard impact is employed.

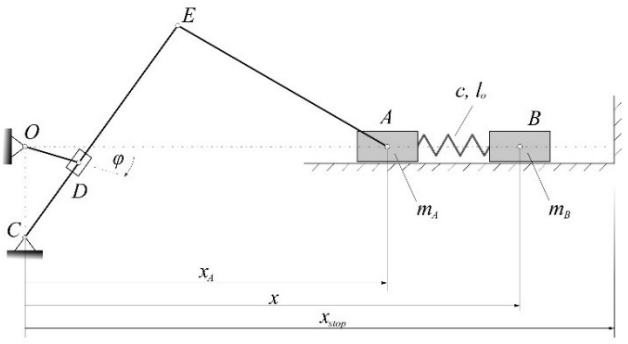

Figure 1. Vibro-impact system.

The mathematical model is derived from Lagrange's equation of motion (Eq. 1):

$$\frac{d}{dt}\left(\frac{\partial E_K}{\partial \dot{q}_\iota}\right) - \frac{\partial E_K}{\partial q_i} + \frac{\partial E_p}{\partial q_i} = Q_{qi} \quad (1)$$

where E_K represents kinetic energy of the system, E_p is potential energy of the system, q_i generalized coordinate, $\dot{q}_\iota$ generalized velocity and Q_{qi} generalized force.

Since the vibro-impact system has one degree of freedom, the motion of the system can be completely described by coordinate the $x(t)$, defining position of the impact element. Lagrange's equation for system shown in Figure 1 with generalized coordinate x is (Eq. 2):

$$\frac{d}{dt}\left(\frac{\partial E_K}{\partial \dot{x}}\right) - \frac{\partial E_K}{\partial x} + \frac{\partial E_p}{\partial x} = Q_x \quad (2)$$

Mathematical model of the vibro-impact is given by Eq. 3:

$$m_B\ddot{x} + c(x - l_o - x_A) = F_f \quad (3)$$

where x_A is position of the piston element and can be expressed as a function of angle of rotation of the electric motor, φ and F_f is the friction force that is calculated for each friction model individually.

The excitation of the vibro-impact system considered in this study is ideal, therefore the kinematics of the drive mechanism is prescribed and does not depend on the motion of the impact element. Motion of the piston element is known in advance as a function of the rotation angle of the electric motor. Consequently, the masses and inertial properties of drive mechanism links do not appear explicitly in the mathematical model of the vibro-impact system.

The focus of the analysis is on the influence of friction models on the dynamic behavior of the vibro-impact system; therefore, several simplifying assumptions were adopted during the modelling process, such as the neglect of air resistance acting on the moving elements.

In this study, the Newton impact model with a coefficient of restitution is chosen to describe the impact between the impact element and rigid barrier. This model is widely used as hard-impact model in the analysis of vibro-impact systems. According to this model, the collision is instantaneous, with negligible contact duration and an instantaneous change in velocity. More complex contact models, such as the viscoelastic model (soft impact) or the Hertz contact model, describe finite contact duration and nonlinear contact stiffness. However, the Newton model provides adequate approximation for theoretical studies on vibro-impact systems focused on the qualitative influence of system parameters.

In various studies combining theoretical and experimental approaches, the importance of appropriate modelling assumptions in engineering systems has been emphasized, such as in the study of PMC-reinforced CFST columns presented in [28].

Coulomb model describes friction force as constant value that is proportional to the normal contact force. Friction force is acting in direction opposite to the relative velocity between two surfaces, in this case opposite to the velocity of impact element, $\dot{x}$. Coulomb model is applied in case of dry contact surface. In case of lubricated contact, viscous model is used to describe friction. Thin liquid film represents barrier between horizontal surface and impact element; therefore, dry friction does not appear. According to this model, friction force is proportional to the relative velocity of contact bodies, $\dot{x}$, with proportional coefficient *b.* Stribeck effect describes transition from static to dynamic friction. According to this model, friction force is a function of velocity. Friction force is decreasing from static friction to Coulomb friction with increasing in velocity. Coulomb-Stribeck model is used to describe more accurate model of friction [1].

Expressions for friction force for Coulomb, viscous and Coulomb-Stribeck model are presented by Eq. (4), Eq. (5) and Eq. (6), respectively.

$$F_f = -\mu m_B g \cdot sign(\dot{x}) \quad (4)$$

$$F_f = -b\dot{x} \quad (5)$$

$$F_f = -\left(\mu + (\mu_s - \mu)e^{-\left|\frac{\dot{x}}{v_s}\right|^\delta}\right) \cdot m_B g \cdot sign(\dot{x}) \quad (6)$$

The key parameter in the Coulomb friction model is the friction coefficient μ, which determines the magnitude of the friction force. Consequently, the level of energy dissipation during motion is directly influenced by the value of the friction coefficient. In the viscous friction model, the rate of the energy dissipation is determined by the damping coefficient *b.* In the Coulomb-Stribeck friction model two key parameters appear: the Stribeck velocity v_s and the exponent δ. The velocity range over which the transition from static to Coulomb friction occurs is characterized by Stribeck velocity v_s, while the

shape of this transition is determined by the exponent δ. Variations of these parameters influence the friction force characteristics, particularly at low relative velocities. Consequently, these parameters can affect the dynamic response of the vibro-impact system, including the occurrence of impact and non-impact behavior.

The parameters of the system used in this dynamical analysis are given in Table 1. The focus of the present study is on the theoretical analysis of a vibro-impact model rather than on a specific engineering device. Therefore, the parameters were chosen to provide framework for exploring the influence of friction modelling on the dynamic behavior of the vibro-impact system with ideal excitation.

Table 1. System parameters.

Parameter	Notation	Value	Unit
Mass of impact body	m_B	*1*	kg
Stiffness of the spring	c	$9\pi^2$	N/m
Length of driver link $\overline{OD}$	r	*0.05*	m
Undeformed length of spring	l_o	*0.4*	m
Distance $\overline{OC}$	l_1	*0.075*	m
Length of bar $\overline{CE}$	l_2	*0.225*	m
Length of bar $\overline{EA}$	l_3	*0.2*	m
Gravitational acceleration	g	*9.81*	m/s^2
Friction coefficient	μ	*0.2*	/
Static friction coefficient	μ_s	*0.5*	/
Damping coefficient	b	*0.2*	Ns/m
Stribeck velocity	v_s	*0.001*	m/s
Stribeck exponent	δ	*1*	/
Coefficient of restitution	k	*0.5*	/
Position of the barrier	x_{stop}	*1.1*	m

3. Dynamic Analysis

To analyze the dynamic behavior of the vibro-impact system amplitude-frequency diagrams are constructed for three different friction models: Coulomb, viscous and Coulomb-Stribeck model. Simulations were performed for *50* s of motion to ensure achievement of the steady state motion and values of maximum and minimum displacements were recorded for different $\Omega p/\omega$ ratio, where Ωp represents angular velocity of the excitation source and ω represents the natural frequency $\omega = \sqrt{c/m_B}$. Diagrams are presented for values of $\Omega p/\omega$ ratio between 0.7 and 1.8. Solutions, noted by red color, represent the numerical solutions for the case of increasing value of $\Omega p/\omega$ ratio, whereas blue values represent the numerical solution for the case of decreasing value of $\Omega p/\omega$ ratio. Top solid green line represents fixed wall in which a sliding body can impact, whereas bottom solid green line represents potential fixed wall. Vertical solid black lines separate regions in diagram for different system behavior.

3.1. Coulomb friction model

The diagram presented in Figure 2 shows the amplitude-frequency diagram for vibro-impact system in case of Coulomb friction model. Diagram shows three different regions: non-impact behavior for $\Omega_p/\omega < 0.87$ and $\Omega_p/\omega > 1.35$, impact behavior for $0.87 \leq \Omega_p/\omega < 1.12$ and multiple solution region for $1.12 \leq \Omega_p/\omega \leq 1.35$. Therefore, the width of the multiple solution region is 0.23. For values Ω_p/ω from multiple solution region the system shows sensitivity to the initial conditions, meaning that the regime of the system can be impact or non-impact, depending on the initial position and initial velocity of the impact element.

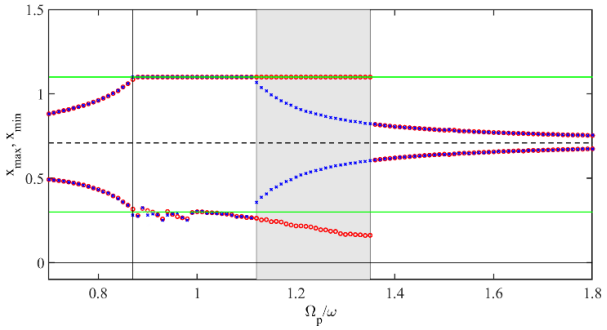

Figure 2. Amplitude-frequency diagram for Coulomb friction model.

For both the non-impact and impact regimes, a representative value of the ratio Ω_p/ω is selected, and the displacement–time responses together with the phase portraits for the steady-state motion are presented in Figure 3 and Figure 4. In the steady-state regime, the system exhibits a displacement amplitude of 0.2637 m and a maximum velocity of 2.008 m/s in the non-impact regime. In the impact regime, the steady-state displacement amplitude increases to 0.404 m, while the maximum velocity reaches 3.8368 m/s. For these system parameters, the number of impacts per excitation period is 1.016 and the impact velocity is equal to 2.3237 m/s.

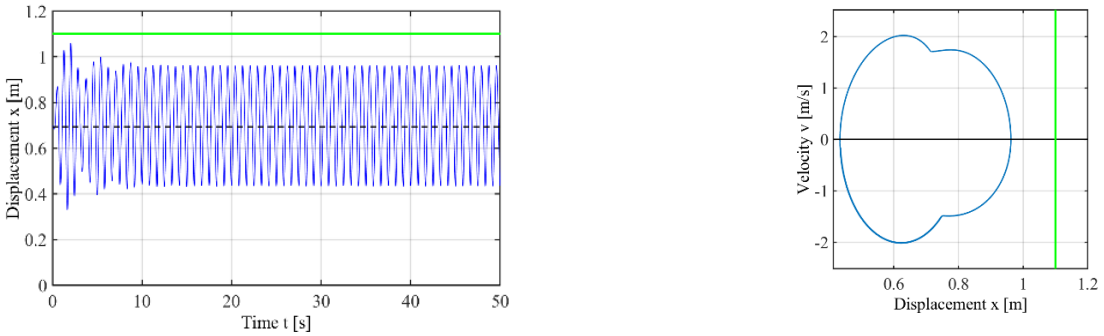

a) b)

Figure 3. System with Coulomb friction model $\Omega_p/\omega = 0.8$: a) displacement-time response; b) phase portrait for steady state motion.

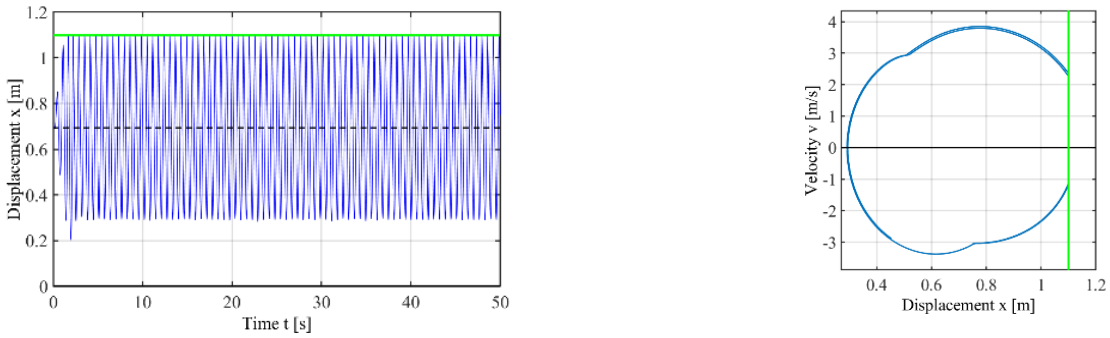

a) b)

Figure 4. System with Coulomb friction model for $\Omega_p/\omega = 1.05$: a) displacement-time response; b) phase portrait for steady state motion.

For specific value of $\Omega_p/\omega = 1.2$ from region with multiple solutions the basin of attraction is presented in Figure 5, to show type of motion dependence on the combination of initial conditions. Combinations of initial conditions, noted by red color, lead to non-impact behavior, while blue color represents combinations for achieving impact behavior. To provide a quantitative description of the basin of attraction, within the considered range of initial conditions the proportion of each region was calculated. Proportion of the impact region of the basin of attraction is approximately 65.76%, while the remaining 34.24% corresponds to the non-impact region. As for the boundary between two regions, it is relatively irregular, indicating a strong sensitivity to the combination of initial conditions near transition region. Combinations of initial conditions close to the boundary may lead to sudden transition between impact and non-impact regime. In material and structural systems, similar nonlinear mechanisms affecting system stability can also be observed. Studies have shown that nonlinear material behavior in composite materials under complex stress states can significantly influence the response and stability of engineering systems [29].

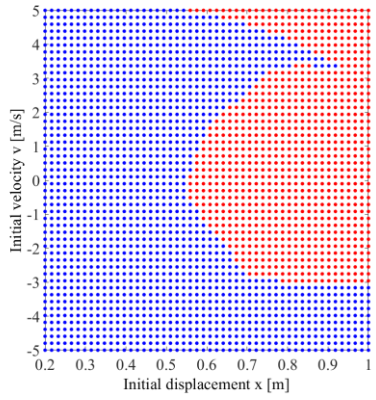

Figure 5. Basin of attraction for system with Coulomb friction model and $\Omega_p/\omega = 1.2$.

Two combinations of initial conditions were selected from two different regions of the basin of attraction shown in Figure 5 in order to construct the displacement–time responses and phase portraits presented in Figure 6.

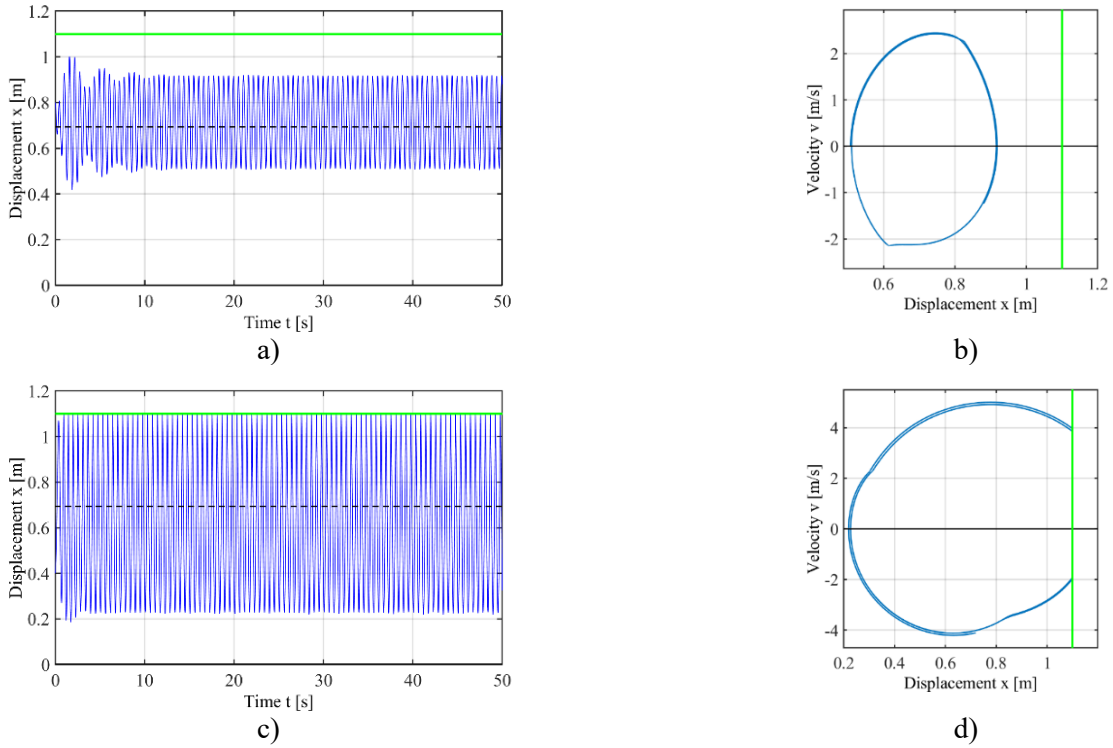

Figure 6. System with Coulomb friction model for $\Omega_p/\omega = 1.2$: a) displacement-time response for $x_o = 0.8$ and $v_o = 0$; b) phase portrait for steady state motion for $x_o = 0.8$ and $v_o = 0$; c) displacement-time response for $x_o = 0.4$ and $v_o = 0$; d) phase portrait for steady state motion for $x_o = 0.4$ and $v_o = 0$.

In the steady-state regime, the displacement amplitude and maximum velocity for the non-impact solution are 0.2052 m and 2.443 m/s, respectively, while for the impact solution they are 0.4407 m and 5.001 m/s, respectively. Number of impacts per excitation period for impact solution is equal to 1.022 and the impact velocity is 3.8765 m/s.

3.2. Viscous friction model

For second friction model – viscous model the amplitude-frequency diagram is presented in Figure 7. Similarly, for the first friction model, diagram shows three different regions: non-impact behavior for $\Omega_p/\omega < 0.87$ and $\Omega_p/\omega > 1.38$, impact behavior for $0.87 \leq \Omega_p/\omega < 1.12$ and multiple solution region for $1.12 \leq \Omega_p/\omega \leq 1.38$. Width of the multiple solution region is 0.26.

To confirm previous amplitude-frequency diagram, two different values of Ω_p/ω were chosen and displacement-time response and phase portrait for the steady state motion are presented in Figure 8 and Figure 9. For the non-impact behavior, the displacement amplitude at steady-state regime is equal to 0.2722 m, while the maximum velocity is 2.2549 m/s. As for the impact regime, during steady-state motion the values of the displacement amplitude and maximum velocity are 0.4066 m and 3.8301 m/s, respectively. Number of impacts per excitation period is 1.016 and impact velocity is 2.4488 m/s.

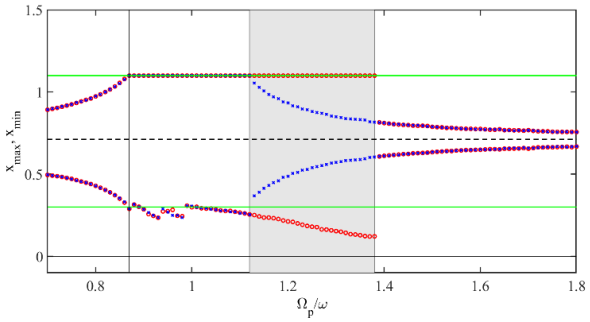

Figure 7. Amplitude-frequency diagram for viscous friction model.

Same as for the first model, for value of $\Omega_p/\omega = 1.2$ from region with multiple solutions, the basin of attraction is presented in Figure 10. As for the viscous friction

model, a quantitative evaluation of the basin of attraction was also performed.

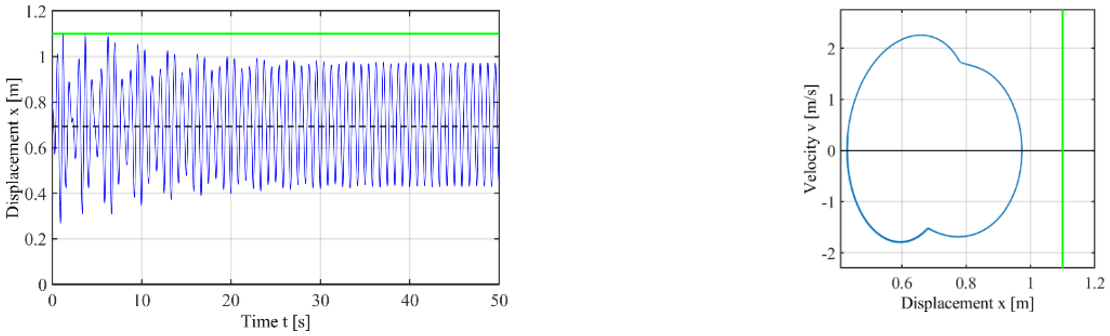

a) b)

Figure 8. System with viscous friction model for $\Omega_p/\omega = 0.8$: a) displacement-time response; b) phase portrait for steady state motion.

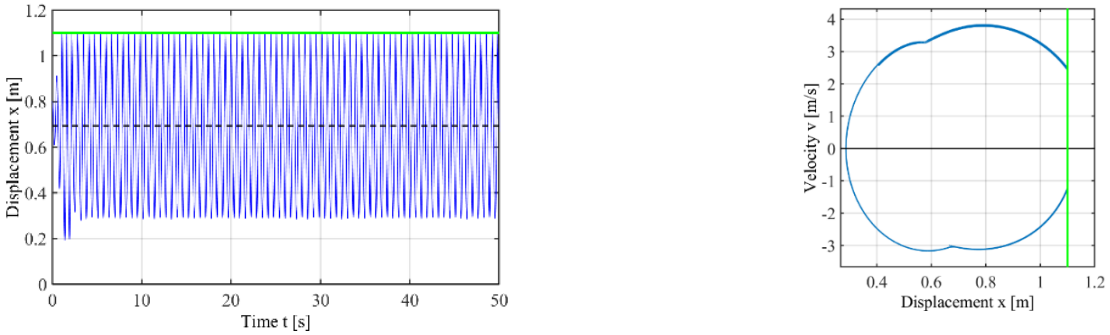

a) b)

Figure 9. System with viscous friction model for $\Omega_p/\omega = 1.05$: a) displacement-time response; b) phase portrait for steady state motion.

The analysis shows that the proportion of the impact region is 85.16%, within the chosen range of initial conditions, while the proportion of the non-impact region is equal to 14.84%. Similarly to the Coulomb friction model, the boundary between two regions is irregular, therefore the system, for combination of initial conditions located close to the boundary, may lead to sudden transition from one region to another.

Displacement-time responses and phase portraits are presented in Figure 11, for combination of initial condition from red and blue region in Figure 10. Based on the displacement-time responses for non-impact and impact solution, the displacement amplitude is equal to 0.2152 m and 0.4415 m, respectively. As for the maximum velocity, for the non-impact motion, it is equal to 2.6495 m/s. For the impact solution, the maximum velocity is equal to 5.0614 m/s and the number of the impacts per excitation period is 1.022. During the steady-state motion, the impact element collides with the fixed barrier at a velocity of 4.0997 m/s.

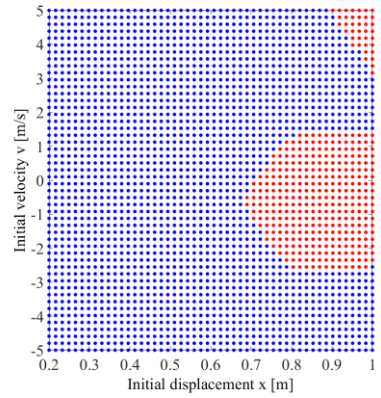

Figure 10. Basin of attraction for system with viscous friction model and $\Omega_p/\omega = 1.2$.

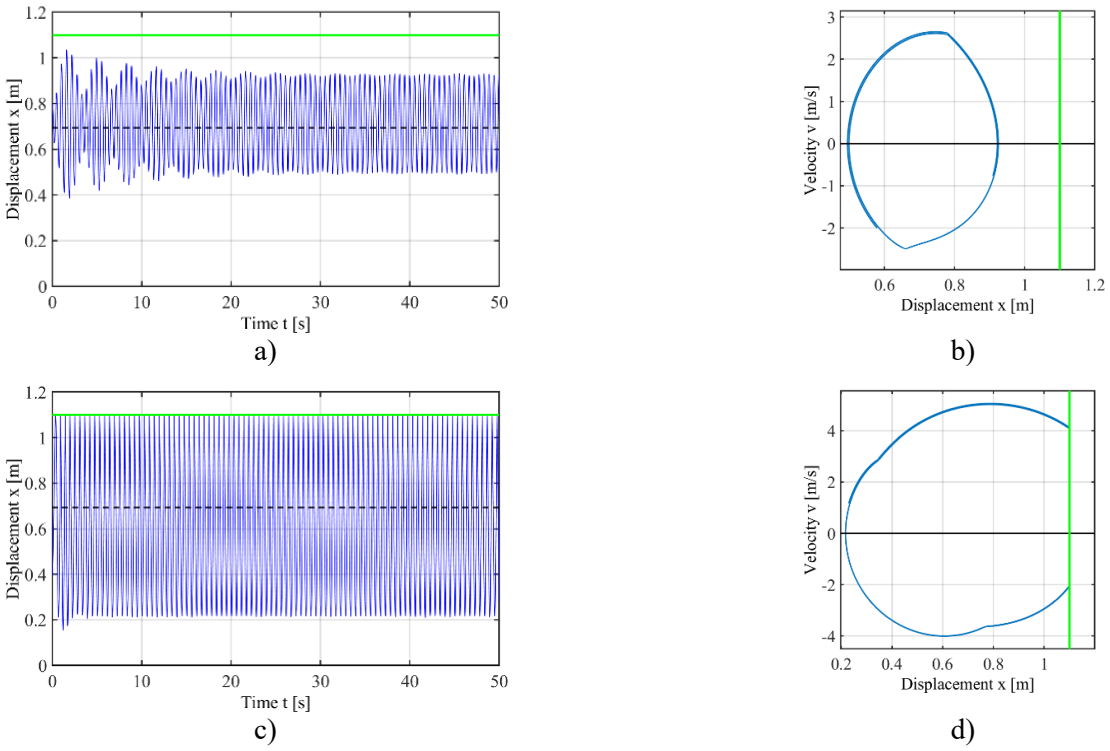

Figure 11. System with viscous friction model for $\Omega_p/\omega = 1.2$: a) displacement-time response for $x_o = 0.8$ and $v_o = 0$; b) phase portrait for steady state motion for $x_o = 0.8$ and $v_o = 0$; c) displacement-time response for $x_o = 0.4$ and $v_o = 0$; d) phase portrait for steady state motion for $x_o = 0.4$ and $v_o = 0$.

3.3. Coulomb-Stribeck friction model

Lastly, amplitude-frequency diagram for system with Coulomb-Stribeck model is presented in Figure 12. Three different regions are shown in amplitude-frequency diagram, therefore behavior of the system is: non-impact for $\Omega_p/\omega < 0.87$ and $\Omega_p/\omega > 1.35$, impact for $0.87 \leq \Omega_p/\omega < 1.12$ and multiple solution region for $1.12 \leq \Omega_p/\omega \leq 1.35$. Based on the amplitude-frequency diagram, the width of the multiple solution region is 0.23.

Displacement-time responses and phase portraits are shown in Figure 13 and Figure 14 for two values of Ω_p/ω – one from non-impact and one from impact region shown on amplitude-frequency diagram. For non-impact solution (Figure 13), the displacement amplitude is 0.264 m and maximum velocity is 2.0173 m/s. In case of impact solution (Figure 14), the values of the displacement amplitude and maximum velocity are 0.4032 m and 3.8291 m/s, respectively. Number of impacts per excitation period is equal to 1.016 and the impact velocity is 2.3211 m/s.

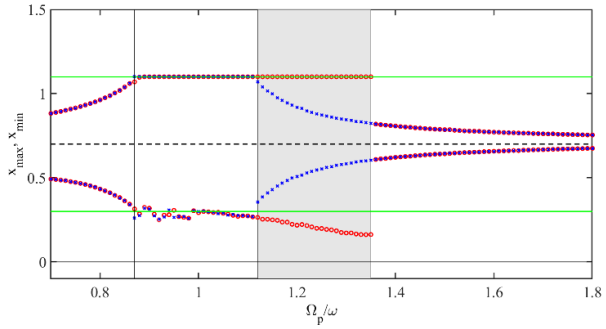

Figure 12. Amplitude-frequency diagram for Coulomb-Stribeck friction model.

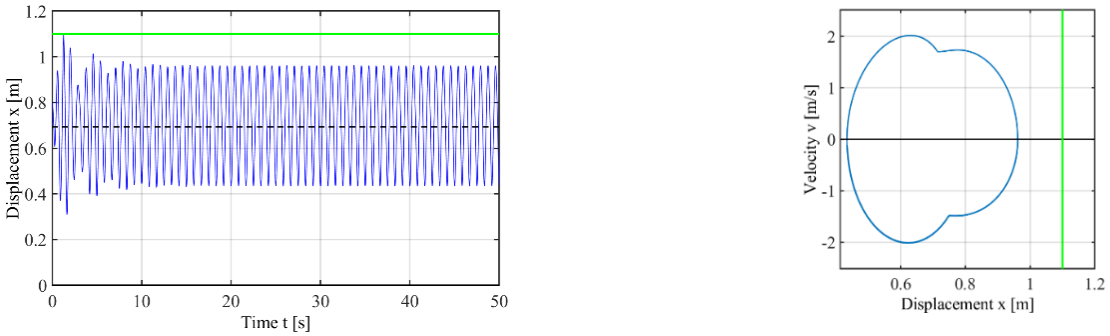

a) b)

Figure 13. System with Coulomb-Stribeck friction model for $\Omega_p/\omega = 0.8$: a) displacement-time response; b) phase portrait for steady state motion.

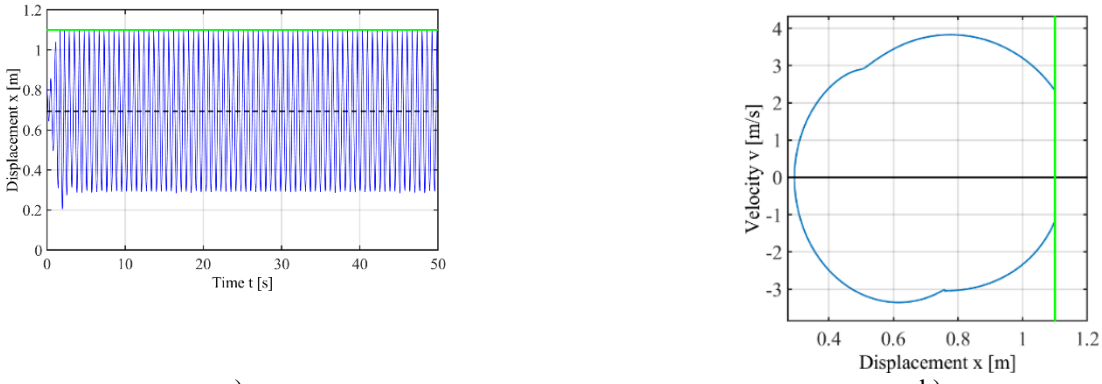

a) b)

Figure 14. System with Coulomb-Stribeck friction model for $\Omega_p/\omega = 1.05$: a) displacement-time response; b) phase portrait for steady state motion.

Basin of attraction for ratio $\Omega_p/\omega = 1.2$ in case of system with Coulomb-Stribeck model is presented in Figure 15. The results of the quantitative analysis show that the proportion of the impact region is 65.6%, while the non-impact region covers the remaining 34.4%, within the chosen combinations of initial conditions.

Displacement-time responses and phase portraits are presented in Figure 16, for combination of initial condition from red and blue region in Figure 15. Same as for the previously shown displacement-time responses and phase portraits the displacement amplitude and maximum velocity are determined. For the non-impact solution these values are 0.2043 m and 2.4266 m/s, while for the impact solution values are 0.4361 m and 4.9602 m/s. During the steady-state motion, the impact velocity is equal to 3.8685 m/s and the number of impacts per excitation period is 1.022.

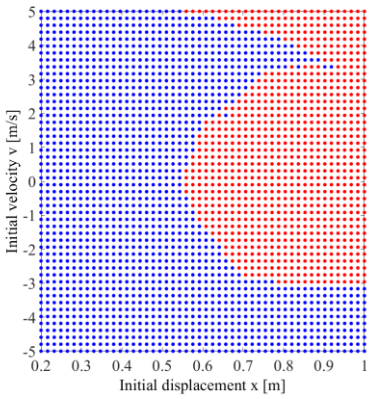

Figure 15. Basin of attraction for system with Coulomb-Stribeck friction model and $\Omega_p/\omega = 1.2$.

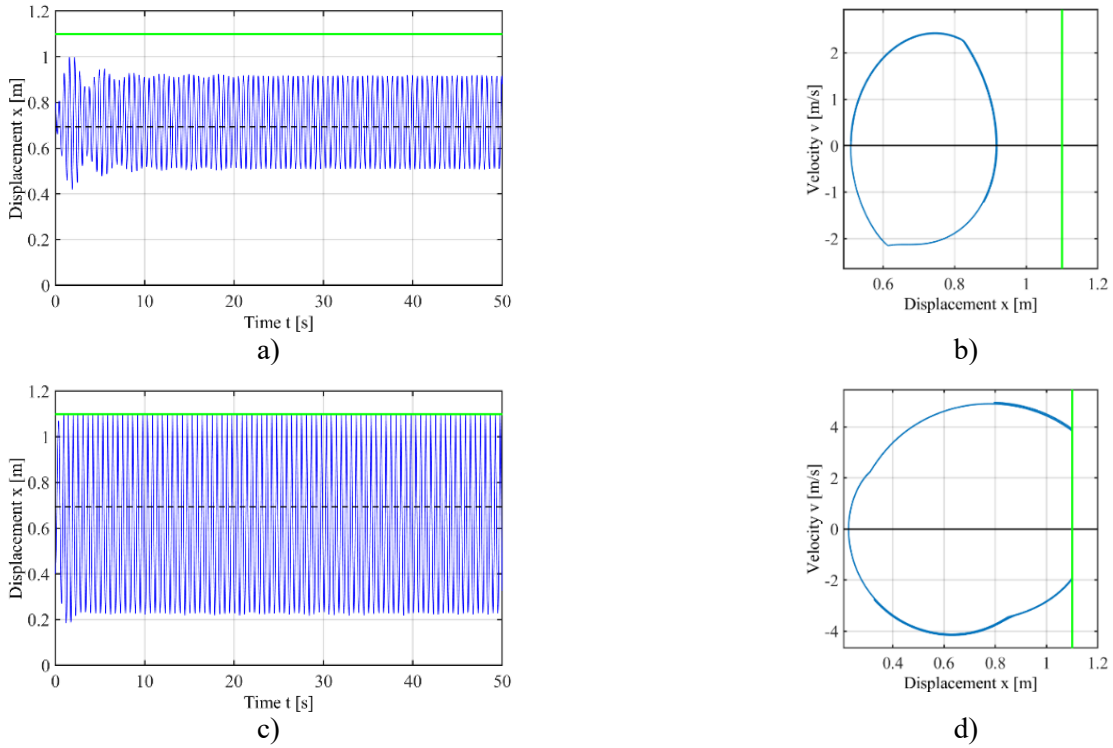

Figure 16. System with Coulomb-Stribeck model for $\Omega_p/\omega = 1.2$: a) displacement-time response for $x_o = 0.8$ and $v_o = 0$; b) phase portrait for steady state motion for $x_o = 0.8$ and $v_o = 0$; c) displacement-time response for $x_o = 0.4$ and $v_o = 0$; d) phase portrait for steady state motion for $x_o = 0.4$ and $v_o = 0$.

4. Conclusion

The influence of different friction models on the dynamic behavior of the vibro-impact system with ideal excitation is analyzed. The system consists of a drive mechanism, a piston and an impact element attached via spring to the piston. The system is driven by an electric motor and in case of ideal excitation the excitation source is not affected by the system dynamics – angular velocity of the electric motor remains constant during the motion. Analysis is performed for three different friction models: Coulomb, viscous and Coulomb-Stribeck model.

Simulations are performed over *50* s of motion for different excitation frequencies and the extreme displacement values in steady-state motion are extracted for each excitation frequency. Results are presented through amplitude–frequency diagrams obtained via run-up and close-down analysis. Three different regions can be distinguished on all three amplitude-frequency diagrams: non-impact, impact and multiple solution region. A key difference in the amplitude–frequency diagrams is that the frequency interval associated with the multiple solution region is wider for the viscous friction model than for the Coulomb and Coulomb–Stribeck models. The width of the multiple solution region for viscous friction model is approximately 13% higher than for case of the Coulomb or Coulomb-Stribeck model. Friction force, in case of viscous friction model, continuously changes with velocity, unlike the Coulomb friction, where the friction force remains constant. As a result of this velocity dependent friction force, the transitions between different dynamical regimes are smoother and the coexistence of multiple attractors becomes more pronounced. Therefore, it expands the region of multiple solutions. The similarity between the Coulomb and Coulomb–Stribeck models can be explained by the fact that the Coulomb–Stribeck friction model approaches Coulomb friction at higher velocities. Value of friction force is nearly constant in this velocity range, which leads to similar dynamic response to the response obtained with Coulomb friction model. The broader multiple solution region observed for the viscous friction model indicates increased sensitivity of the system to initial conditions. Consequently, small variations of initial conditions may result in a transition from impact to non-impact oscillatory motion.

In both the non-impact and impact regions, the system response is independent of the initial conditions. Two excitation frequencies are selected: one corresponding to the non-impact region and one to the impact region and displacement-time responses and phase portraits at steady-state motion are presented for three different friction models. For the chosen value of the excitation frequency from non-impact region, the displacement amplitudes and maximum velocities are determined for each friction model. In case of viscous friction model, the displacement amplitude is approximately 3.2% higher than the amplitude obtained for Coulomb model, while the difference between Coulomb and Coulomb-Stribeck models is negligible (about 0.1%). The viscous friction model also leads to the maximum velocity during the steady-state motion, which is approximately 12% higher than for the other two friction models. In case of excitation frequency from impact region for all three friction models, the differences in steady-state displacement amplitudes and maximum velocities are relatively small, while the number of impacts per excitation period is approximately 1.016. Noticeable difference is observed in the impact velocity: the viscous friction model leads to approximately 5.3% higher mean impact velocity than mean impact velocity for Coulomb model and slightly higher than for the Coulomb–Stribeck model.

In the multiple solution region, the system response depends strongly on the initial conditions. Therefore, the system for the same value of the excitation frequency can collide with the fixed barrier or oscillate without impacts with the barrier. For a specific value of the excitation frequency for each friction model, the basin of attraction is constructed to describe the dependence on the initial conditions. For each employed friction model, two regions can be noted on the basin of attraction: combinations that lead to non-impact behavior and combinations that lead to impact behavior. The diagrams exhibit a similar qualitative structure for all three models, with a distinct boundary separating the two regions clearly visible. Quantitatively, the basins of attraction show significant differences in the proportion of each region – impact and non-impact. The viscous friction model leads to the largest proportion of the impact region in the basin of attraction (85.16%) within the chosen range of initial conditions, while the Coulomb and Coulomb-Stribeck friction models exhibit considerably smaller impact regions (65.76% and 65.6%, respectively).

A combination of initial conditions is selected from each region, and the corresponding diagrams are presented for each friction model. The corresponding displacement–time responses and phase portraits confirm the predicted non-impact and impact behaviors at steady-state motion. Results for the non-impact solution confirm the previous conclusions for non-impact region, that the viscous friction model leads to higher displacement amplitude and maximum velocity than the Coulomb and Coulomb-Stribeck model. In case of the impact solution a similar tendency, as for the impact region, can be observed. For all three friction models, the displacement-time amplitudes and maximum velocities remain very close, while the number of impacts per excitation period remains practically the same. A noticeable difference appears in the mean impact velocity – the highest value is observed for the viscous friction model.

Obtained results indicate that systems operating under conditions that can be described by viscous friction, for example lubricated contacts, exhibit a wider multiple solution region. Therefore, over a wider interval of excitation frequency the system shows a strong dependence on the initial conditions. When such friction conditions are present, it is necessary to carefully select the initial conditions in order to avoid sudden transitions between non-impact and impact motion. In the case of dry contact conditions, which can be described by Coulomb or Coulomb–Stribeck friction models, the vibro-impact system exhibits a narrower multiple solution region. This leads to a more predictable dynamic behavior of the system. If stable impact motion is required for a mechanical system, such friction conditions may provide more reliable operating conditions. The results of the analysis also show that in the case of the viscous friction model the impact velocities are higher than for the Coulomb and Coulomb–Stribeck models. In engineering applications this may be advantageous in situations where higher kinetic energy transfer during impact is desirable. However, higher impact velocities may also lead to larger dynamic loads and increased wear of the vibro-impact system components. Based on the basin of attraction analysis, combinations of initial conditions located close to the boundary between the regions should be avoided, since small variations may result in transitions between different motion regimes. Such transitions may lead to difficulties in predicting the system response.

The present study analyzes a single-degree-of-freedom vibro-impact system with ideal excitation. Mechanical

systems often exhibit multiple degrees of freedom in practical applications, while the non-ideal excitation introduces an additional degree of freedom. Furthermore, in the present study all components of the system are considered rigid. Considering systems with multiple degrees of freedom, non-ideal excitation, and structural flexibility would significantly increase the complexity of the mathematical model and consequently the dynamic analysis.

Future research will be directed toward the analysis of the vibro-impact system with non-ideal excitation. Such type of excitation significantly contributes to the nonlinearity of the system and potentially expands the regions of complex behavior. Furthermore, different impact models will be considered, including models that describe the contact interaction through a continuous force–deformation relationship acting over a finite time interval, unlike the Newton restitution law, which assumes an instantaneous velocity change at the moment of impact. A comprehensive bifurcation analysis will also be performed in order to identify and classify various dynamical regimes, including periodic, quasi-periodic and chaotic responses, as well as transitions between them. These investigations will contribute to a deeper understanding of the nonlinear phenomena governing vibro-impact systems and provide guidelines for their reliable operation and control.

Competing Interest Statement

The authors declare no known competing financial interests or personal relationships that could have influenced the work reported in this study.

Data Availability Statement

Supplementary materials and data used in this research are accessible upon request. For access, please contact the corresponding author via kanita.lemes@mef.unsa.ba.

References

[1] Lemes K., Hajradinovic Dz., Petrovic M., "Numerical Analysis of a Nonlinear Vibrating Two Degrees-of-Freedom System with Various Friction Models," *International Research Journal of Innovations in Engineering and Technology,* vol. 4, no. 3, pp. 6-12, 2020.

[2] van Geffen V., A study of friction models and friction compensation, Eindhoven: Technische Universiteit Eindhoven, 2009.

[3] Liu Y.F., Li. J., Zhang Z.M., Hu X.H., Zhang W., "Experimental comparison of five friction models on the same test-bed of the micro stick-slip motion system," *Mechanical Sciences ,* vol. 6, no. 1, pp. 15-28, 2015.

[4] Hajradinović Dž., Zuković M., Kovačić I., "Influence of the stall torque on a vibro-impact system with non-ideal excitation," in *2nd International E-Conference on Advances in Engineering, Technology and Management - ICETM*, 2020.

[5] Hajradinovic Dz., Zukovic M., "Different Solutions Of A Vibro-Impact System with Non-Ideal Excitation Based on the Misalignment of Frequency Response Curves Obtained by A Numerical and Analytical Analysis," *International Journal of Mechanical Engineering,* vol. 7, no. 1, 2022.

[6] Zuković M., Hajradinović Dž., Kovačić I., "On the dynamics of vibro-impact systems with ideal and non-ideal excitation," *Meccanica,* vol. 56, p. 439–460, 2021.

[7] Zukovic M., Hajradinovic Dz., Kovacic I., "Vibro-impact system with non-ideal excitation: analytical investigations," *Nonlinear Dynamics ,* vol. 106, pp. 105-123, 2021.

[8] Liu Y., Pavlovskaia E., Hendry D., Wiercigroch M., "Vibro-impact responses of capsule system with various friction models," *International Journal of Mechanical Sciences,* vol. 72, p. 39–54, 2013.

[9] Liu Y., Wiercigroch M., Pavlovskaia E., Yu H., "Modelling of a vibro-impact capsule system," *International Journal of Mechanical Sciences,* vol. 66, pp. 2-11, 2013.

[10] Liu Y., Jiang H., Pavlovskaia E., Wiercigroch M., "Experimental Investigation of the Vibro-impact Capsule System," *Procedia IUTAM,* vol. 22, pp. 237-243, 2017.

[11] Liu Y., Pavlovskaia E., Wiercigroch M., "Experimental verification of the vibro-impact capsule model," *Nonlinear Dynamics,* vol. 83, p. 1029–1041, 2016.

[12] Liu Y., Pavlovskaia E., Wiercigroch M., Peng Z., "Forward and backward motion control of a vibro-impact capsule system," *International Journal of Non-Linear Mechanics,* vol. 70, pp. 30-46, 2015.

[13] Nguyen K.T., La N.T., Ho K.T., Ngo Q.H., Chu N.H., Nguyen V.D., "The effect of friction on the vibro-impact locomotion system: modeling and dynamic response," *Meccanica,* vol. 56, p. 2121–2137, 2021.

[14] La N.T., Nguyen T.T., Nguyen V.D., "A comparative study on the two vibration driven locomotion systems in various friction levels," *Vietnam Journal of Mechanics,* vol. 43, no. 2, p. 121–137, 2021.

[15] de Souza S.L.T., Caldas I.L., Viana R.L., Balthazar J.M., Brasil R.M.L.R.F., "Basins of attraction changes by amplitude constraining of oscillators with limited power

supply," *Chaos, Solitons and Fractals,* vol. 26, p. 1211–1220, 2005.

[16] Pavlovskaia E., Hendry D.C., Wiercigroch M., "Modelling of high frequency vibro-impact drilling," *International Journal of Mechanical Sciences,* vol. 91, pp. 110-119, 2015.

[17] Liu Y., Chavez J.P., Guo B., Birler R., "Bifurcation analysis of a vibro-impact experimental rig with two-sided constraint," *Meccanica,* vol. 55, p. 2505–2521, 2020.

[18] Liu R., Niu J., Shen Y., Yang S., "Stability and bifurcation analysis of two-degrees-of-freedom vibro-impact system with fractional-order derivative," *International Journal of Non-Linear Mechanics,* vol. 126, 2020.

[19] Piccirillo V., "Suppression of chaos in nonlinear oscillators using a linear vibration absorber," *Meccanica,* vol. 56, p. 255–273, 2020.

[20] de Souza S.L.T., Caldas I.L., Viana R.L., "Damping control law for a chaotic impact oscillator," *Chaos, Solitons & Fractals,* vol. 32, p. 745–750, 2007.

[21] Luo G.W., Lv X.H., "Controlling bifurcation and chaos of a plastic impact oscillator," *Nonlinear Analysis: RealWorld Applications,* vol. 10, p. 2047–2061, 2009.

[22] de Souza S.L.T., Caldas I.L., Viana R.L., Balthazar J.M., Brasil R.M.L.R.F., "Impact dampers for controlling chaos in systems with limited power supply," *Journal of Sound and Vibration,* vol. 279, p. 955–967, 2005.

[23] Stefani G., De Angelis M., Andreaus U., "Scenarios in the experimental response of a vibro-impact single-degree-of-freedom system and numerical simulations," *Nonlinear Dynamics,* vol. 103, p. 3465–3488, 2021.

[24] Stefani G., De Angelis M., Andreaus U., "Influence of the gap size on the response of a single-degree-of-freedom vibro-impact system with two-sided constraints: Experimental tests and numerical modeling," *International Journal of Mechanical Sciences,* vol. 206, 2021.

[25] Mann B.P., Carter R.E., Hazra S.S., "Experimental study of an impact oscillator with viscoelastic and Hertzian contact," *Nonlinear Dynamics,* vol. 50, p. 587–596, 2007.

[26] Okolewski A., Blazejczyk-Okolewska B., "Hard versus soft impact modeling of vibro-impact systems with a moving base," *Nonlinear Dynamics,* vol. 105, p. 1389–1403, 2021.

[27] Luo L., Li Y., Dai H., Sun H., Jia M., Yuan H., Cheng X., "Seismic performance prediction and interpretation of RC bridges under vehicle-bridge interaction: From VBI system simulation to ensemble learning surrogate models," *Engineering Structures,* vol. 341, 2025.

[28] Luo L., Sun H., Jia M., Peng B., Li X., Yuan H., Liu G., , "Experimental study and theoretical prediction of axial compression behavior in PMC-reinforced CFST columns with void defects," *Engineering Structures,* vol. 313, 2024.

[29] Luo L., Shi J., Wang J., Qu Y., Dai B., "Experimental study on flexural performance of ultra-high-performance concrete with recycled aggregate co-modified by nano-silica and steel fiber," *Construction and Building Materials,* vol. 411, 2024.